Precision Stark spectroscopy of sodium ^2P and ^2D states

J. F. Baugh, C. E. Burkhardt, and J. J. Leventhal
Department of Physics, University of Missouri–St. Louis, St. Louis, Missouri 63121-4499

T. Bergeman
Department of Physics and Astronomy, State University of New York at Stony Brook, Stony Brook, New York 11794-3800
(Received 13 January 1998; revised manuscript received 6 April 1998)

We report precision measurements of the energies of the Na $10\,^2P$, $11\,^2P$, and $10\,^2D$ states and their fine-structure intervals. The P-state results bridge the gap between earlier high- and low-n measurements from other laboratories, thus facilitating calculation of quantum-defect parameters. Quantum-defect theory fits to all available data on Na are critically examined. Using the most reliable values at low, intermediate, and high n leads to a single set of four quantum-defect parameters that is useful over the entire range of n. Also, using the present P-state measurements, we extract a value of the ionization potential that is in exact agreement with our earlier determination. [S1050-2947(98)08308-5]

PACS number(s): 32.30.Bv, 32.60.+i, 32.80.Rm, 32.10.Hq

Although the principal series of sodium has been studied for many years, precision measurements of the ^2P energies have been made only for $n \lesssim 7$ and $22 \gtrsim n \gtrsim 32$. Quantum defects deduced from these two sets of measurements should agree, but this was not the case. Our earlier attempt [1] to combine all then available data [2–11] to fit quantum defects for this manifold revealed that, on the stated levels of experimental accuracy, these low-n and high-n measurements were incompatible.

In an effort to resolve the discrepancy we performed experiments using constant energy Stark spectroscopy, the data from which lead to precision determinations of the binding energies and fine-structure splittings in the crucial range of $n \sim 8-12$ that bridges the gap between the high- and low-n measurements. Our measurements of the $10\,^2P$ and $11\,^2P$ energies and fine-structure intervals indicate that certain high-n measurements, acquired from microwave (mw) experiments prior to 1995 [4], suffered from small but significant Stark shifts that account for the incompatibility. More recent mw data [12,13] are, however, in substantial agreement with our conclusion.

Our previous study [1] showed the usefulness of accurate intermediate energy-level binding energies when fitting combined mw and optical data. Normally, spectroscopic transition frequencies give only energy differences and thus require a fit of many such data to obtain the quantum defect of a single level. Using constant energy Stark spectroscopy, however, we determine the binding energy. Thus the quantum defect of a level can be obtained from a single measurement. Moreover, from the binding energies the ionization potential of the ground state atom can also be calculated [1].

The essence of our method is to excite a high-lying state, say, $n \gtrsim 20$, by stepwise transitions, the last transition of which is effected with a very accurately known laser line, a CO_2 line [14] in this work. The upper-level energy of the last transition can be accurately deduced by comparison with calculated Stark sublevel energies. The binding energy of the lower level is then found by adding the energy of the CO_2 laser line. Most sublevels of the high-n state are hydrogenic, so existing quantum-defect parameters suffice, possibly with rapidly converging iterative refinement. We combine our measured energies with all available sodium spectroscopy data in a general fit of quantum-defect parameters.

The apparatus [1] provided a beam of sodium atoms, density $\approx 10^7$ cm^{-3}, that was irradiated by two or three laser beams at the center of a pair of Stark plates to which a dc electric field F was applied. The intermediate $10\,^2P$ and $11\,^2P$ states were excited by ultraviolet laser light obtained by frequency doubling the output of a grazing incidence dye laser pumped by a 10-Hz Nd:YAG laser (where YAG denotes yttrium aluminum garnet). The intermediate $10\,^2D$ state was excited in two steps through the $3\,^2P$. The atoms were also irradiated by a CO_2 laser beam tuned to a specific CO_2 line. The gain curve of the CO_2 laser is ≈ 100 MHz wide, so that, although tuned manually to the maximum of the gain curve, there was roughly a 15-MHz uncertainty in the photon energy of the CO_2 laser beam.

The Stark field F was applied to the plates prior to the laser pulses and increased about 1 μsec after the laser pulse to a value sufficient to ionize highly excited atoms, but not atoms in intermediate states. These ions were detected and F spectra acquired by scanning F stepwise over symmetric values, minus to plus, and recording the ion signal at each setting. This technique requires no absolute field calibration and assumes only that the electric-field scan is linear.

From the F spectra, the resonance fields were obtained by fitting each peak with a Gaussian line shape, using multiple overlapping peaks where appropriate. Peaks at positive and negative fields were averaged to eliminate the effect of any voltage offsets (maximum 80 mV/cm) and then the resonance voltages fit to calculated Stark sublevel energies as in Ref. [1] to obtain two upper-level energies and a field calibration parameter (effective plate spacing). For blended lines, an unweighted average was used. Figure 1 displays the F spectrum used to obtain the binding energy of $11\,^2P$. The linewidth of the ultraviolet laser produced excitation from both fine-structure levels of the lower ^2P states and accordingly two sets of peaks are identifiable in the spectra.

In our Stark calculations, the energy is given by $E(n,L,J) = R_{\mathrm{Na}}/[n - \delta(n,L,J)]^2$. Here $R_{\mathrm{Na}} = R_\infty \rho_{\mathrm{Na}}$, with

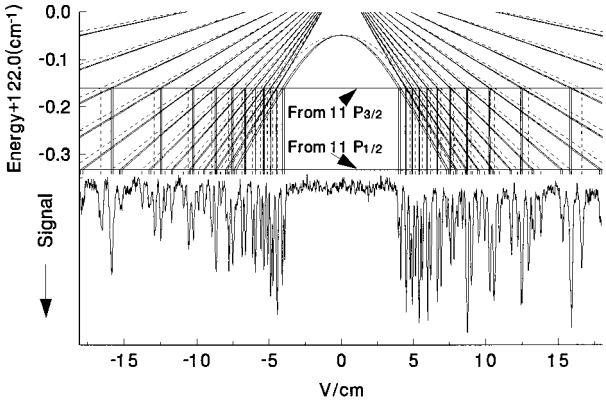

FIG. 1. F spectrum obtained by exciting the Na 11 ^2P_J states by the CO_2 $10P(20)$ laser line (bottom), together with a plot of calculated energies of Stark sublevels from $n=30$ (top). $|m_J|=1/2$ levels are shown as solid lines, $|m_J|=3/2$ levels as dashed lines. The fitted upper-level energies corresponding to excitation from each of the two lower fine-structure levels are shown as horizontal lines. The locations of these lines together with the Stark energies give the calculated positions of the resonances, as indicated by vertical lines.

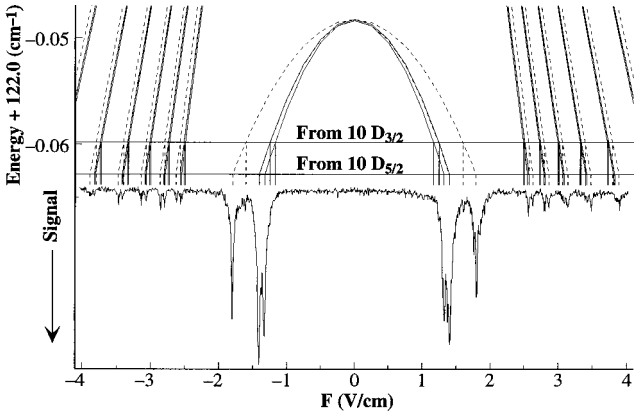

FIG. 2. F spectrum, as in Fig. 1, obtained by exciting the Na $10\,^2D_J$ states by the CO_2 $10R(24)$ line (bottom), together with Stark sublevel energies from the $n=30$ manifold (top). One very small resolved peak from the $10\,^2D_{3/2}$ level occurs at 1.6 V/cm, while all other peaks are predominantly from the $10\,^2D_{5/2}$ level.

$R_\infty = 109\,737.315\,683\,7(31)$ cm^{-1} from recent spectroscopy of hydrogen [15,16] and $\rho_{\rm Na}=M/(M+m_e)=1-m_e/M_A$ [17], where $M=M_{\rm Na}-m_e$ is the mass of the sodium ion core, $M_{\rm Na}$ the mass of the neutral sodium atom, and m_e the electron mass. This yields $R_{\rm Na}=109\,734.6972$ cm^{-1}. The quantum defect is represented by the iterative expression

$$\delta(n,L,J)=a_0+a_1t+a_2t^2+a_3t^3+\cdots, \qquad (1)$$

where $t=1/[n-\delta(n,L,J)]^2$ is the energy in rydbergs and the coefficients a_i depend on L and J. With this form, the a_i are most easily interpreted [18].

Stark sublevel energies were computed by diagonalizing a matrix in a basis of n, L, and J states, following Zimmerman *et al.* [19], using wave functions computed with $r^{1/2}$ scaling [20]. A sufficient number of basis states (Table I) were included for convergence to 0.5 MHz up to $F\approx 20$ V/cm. The polarizability of the lower state, calculated by the same means, was included but had no significant affect. The quantum-defect parameters needed for computing the upper level Stark energies were obtained from the fit to the spectroscopic data for $L\leqslant 5$ and from the dipole and quadrupole polarizabilities and from the hydrogenic relativistic mass correction and spin-orbit effects [21,7] for $L>5$. The experimentally deduced parameters were updated using our results, but no significant change in the calculated energies resulted.

Two fitted energies correspond to excitation from the two lower fine-structure components. The fitted energies for the $n=10$ and 11 $^2P_{1/2}$ and $^2P_{3/2}$ levels obtained from our analysis are given in Table I. The $10\,^2P$ error limits are larger because of line blending as shown in Fig. 1.

For the $10\,^2D$ state, the F spectra, shown in Fig. 2, had linewidths less than 20 MHz, yielding improved binding energies. Since excitation was from $3\,^2P_{3/2}$, $10\,^2D_{5/2}$ is most prominently excited, but there is one weak resolved resonance at about 1.6 V/cm, from excitation of $10\,^2D_{3/2}$. From this, the fine-structure interval is deduced to be 90(6) MHz, in agreement with the quantum-beat spectroscopy value of 91.5 ± 1.5 MHz [22]. The $10\,^2D$ binding energies given in Table I supersede those given in Ciocca *et al.* [1].

The $10\,^2P$ and $11\,^2P$ energies were combined with all published spectroscopic data on sodium to fit quantum-defect parameters for $0\leqslant L\leqslant 5$ for $J=L\pm 1/2$. Two fits were performed. In the first, all published data were included. For the second, data with residuals greater than four times the estimated experimental error were dropped, as were all the mw

TABLE I. Intermediate sodium atomic level that is the lower level for the CO_2 laser transition, the CO_2 laser wave number, the n range of the n, L, and J basis states used in the Stark level calculation, the fitted upper-state binding energy, and the binding energy of the lower level, obtained by adding the previous two figures. All energies are in cm^{-1}.

Atomic level	CO_2 Laser Line	Energy[a]	Basis states n	Fitted upper-level energy	Lower-level energy	Lower-level energy (fit)
$10\,^2P_{1/2}$	$9R(32)$	1085.7654	19–25	−226.8756(8)	−1312.6410(8)	−1312.6432
$10\,^2P_{3/2}$	$9R(32)$	1085.7654	19–25	−226.6424(8)	−1312.4078(8)	−1312.4094
$11\,^2P_{1/2}$	$10P(20)$	944.1940	26–34	−122.3323(5)	−1066.5263(5)	−1066.5262
$11\,^2P_{3/2}$	$10P(20)$	944.1940	26–34	−122.1599(5)	−1066.3539(5)	−1066.3548
$10\,^2D_{3/2}$	$10R(24)$	978.4723	26–34	−122.0599(5)	−1100.5322(5)	−1100.5326
$10\,^2D_{5/2}$	$10R(24)$	978.4723	26–34	−122.0629(5)	−1100.5352(5)	−1100.5357

[a]Reference [14].

TABLE II. Quantum-defect parameters for Na ^2P states from previous work and from our least-squares fit to available Na spectroscopic data.

State	Ref.	a_0	a_1	a_2	a_3
$^2P_{1/2}$	[9]	0.8554092	0.112453	0.048139	0.03999
$^2P_{1/2}$	[4]	0.855424(6)	0.1222(2)		
$^2P_{1/2}$	[12]	0.85544502(15)	0.112067(86)	0.0479(13)	0.0457(43)
$^2P_{1/2}$	[a]	0.85544502(51)	0.11200(13)	0.0489(19)	0.0426(59)
$^2P_{1/2}$	[b]	0.85544520(31)	0.11190(11)	0.0503(16)	0.0383(48)
$^2P_{3/2}$	[9]	0.8546296	0.111669	0.058813	0.01313
$^2P_{3/2}$	[4]	0.854608(3)	0.1220(2)		
$^2P_{3/2}$	[12]	0.85462615(12)	0.112344(67)	0.0497(10)	0.0406(34)
$^2P_{3/2}$	[a]	0.85462614(51)	0.11232(13)	0.0496(19)	0.0417(61)
$^2P_{3/2}$	[b]	0.85462608(29)	0.112360(69)	0.0491(11)	0.0434(36)

[a]This work. All published data are used. The variance is equal to 5.13.
[b]This work. Outlying data are excluded. The variance is equal to 1.65.

$^2S \rightarrow {}^2P$ data in Refs. [4,5,23], in light of the finding in Refs. [9,10]. Parameters for the ^2S manifold in each case were close to those published in Ref. [1] and those for $2 \leqslant L \leqslant 5$ are close to those given in Ref. [24]. The results for the ^2P parameters are given in Table II along with previous results. The differences in the results between our fits *a* and *b* are indicative of the sensitivity to outlying data.

Table I gives energies calculated from the fitted quantum-defect parameters (fit *b*). We believe the relatively large residuals for 10 ^2P result from blending of resonances, shown in Fig. 1, which makes a precise determination difficult without a detailed theory of the excitation process. For the other two data sets, there was considerable blending, but a few unblended lines made the analysis more precise.

Figure 3 is a representation of the data for the ^2P_J manifolds. Plotted are the ''experimental'' values of $\delta(n,L,J)$ minus the values of $\delta(n,L,J)$ obtained from the parameters in Table II. In the fits to the quantum-defect parameters, experimental transition frequencies were used and the ^2P quantum defects were obtained from both $^2S \rightarrow {}^2P$ and $^2P \rightarrow {}^2D$ transitions and our *F* spectra. The $^2S \rightarrow {}^2P$ frequencies were added or subtracted from the calculated ^2S term energies to obtain $\delta(n,L,J) = \sqrt{R_{\mathrm{Na}}/E(n,L,J)}$. [For our data, $\delta(n,L,J)$ was obtained from the binding energy.] The error bars represent $|\sigma(\delta)| = |\delta\sigma(E)/2E|$, where $\sigma(E)$ is the uncertainty in the frequency measurement. Thus the ^2S energies are assumed to be known exactly. In fact, the ^2S quantum-defect parameters do have smaller uncertainties than the ^2P parameters (the two-photon $n\,{}^2S \rightarrow n'\,{}^2S$ observations of [6] are a factor).

An extrapolation based on two quantum-defect parameters for each *J* manifold given in [12] fits the data well down to $n \sim 8$, but deviates sharply for the lower states, as shown by the deviation of the solid lines from zero. Four-parameter fits represent $^2P_{1/2}$ and $^2P_{3/2}$ data (except the earlier mw data) to within twice the quoted experimental uncertainty or better.

The inset in Fig. 3 is a plot of quantum defect versus binding energy (rather than *n*). It illustrates the value of precision measurements in the range $n \sim 8-12$ and thus additional motivation for the present study. The lowest-energy ''point'' (highest *n*) actually represents *all* of the mw measurements. Only the lowest two quantum-defect parameters (a_0 and a_1) can be obtained from these data [12,13], principally because the energy range spanned is very small. To illustrate, the energy range covered in the present work, $\approx 190\ \mathrm{cm}^{-1}$, is nearly twice that of the recent mw experi-

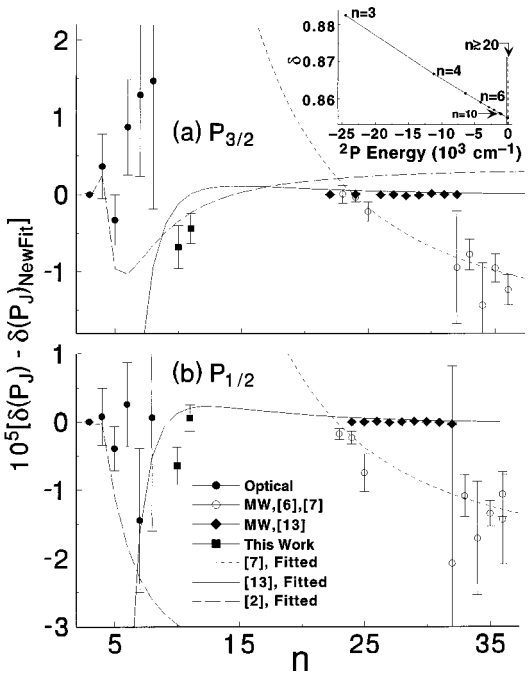

FIG. 3. Survey of available data on Na ^2P states, together with results of quantum defect parameter fits. For optical and microwave transition data, the experimental quantum defects are obtained by adding observed transition energies to fitted ^2S state energies, as discussed in the text. In each case, the plotted values are the differences between measured or calculated quantum-defect parameters and the results of our least-squares fit *b* (Table II). The optical data are from Refs. [5] and [6]. Several outlying points from Ref. [18] have been omitted. The inset is a plot of the quantum defect versus binding energy.

ments. The binding energies presented here, combined with other optical, laser, and interferometric data, make it possible to fit two additional quantum-defect parameters for each fine-structure manifold and thereby estimate other energy levels to a high degree of accuracy.

Using our binding energy measurements in conjunction with accurately known intervals, we calculate the ionization potential of neutral ground-state sodium. This was done in our previous work [1], but the calculation employs a different pathway to ionization. Using our ^2P data and those of Refs. [7,8,12] that were not included in Ref. [1] we obtain an ionization energy of 41 449.451(2) cm^{-1}, in exact agreement with our previous value. Thus we have two different determinations, both of which lead to identical ionization potentials. This is significant because it implies that the sets of quantum-defect parameters for each of $L=0$, 1, and 2 are self-consistent.

The work at the University of Missouri–St. Louis was supported in part by a NSF grant. T.B. gratefully acknowledges support from a UMSL research grant.

[1] M. Ciocca, C. E. Burkhardt, J. J. Leventhal, and T. Bergeman, Phys. Rev. A **45**, 4720 (1992).
[2] T. F. Gallagher, R. M. Hill, and S. A. Edelstein, Phys. Rev. A **13**, 1448 (1976).
[3] T. F. Gallagher, R. M. Hill, and S. A. Edelstein, Phys. Rev. A **14**, 744 (1976).
[4] C. Fabre, S. Haroche, and P. Goy, Phys. Rev. A **18**, 229 (1978); **22**, 778 (1980).
[5] P. Goy, C. Fabre, M. Gross, and S. Haroche, J. Phys. B **13**, L83 (1980).
[6] P. Juncar, J. Pinard, J. Hamon, and A. Chartier, Metrologia **17**, 77 (1981).
[7] L. G. Gray, X. Sun, and K. B. MacAdam, Phys. Rev. A **38**, 4985 (1988).
[8] X. Sun and K. B. MacAdam, Phys. Rev. A **49**, 2453 (1994).
[9] P. Risberg, Ark. Fys. **10**, 583 (1956).
[10] I. Johansson, Ark. Fys. **20**, 135 (1961).
[11] K. W. Meissner and K. F. Luft, Ann. Phys. (Leipzig) **29**, 698 (1937).
[12] S. Dyubko, M. Efimenko, V. Efemov, and S. Podnos, Kvant. Elektron. (Moscow) **22**, 946 (1995) [Quantum Electron. **25**, 914 (1995)].
[13] S. Dyubko, M. Efimenko, V. Efremov, and S. Podnos, Phys. Rev. A **52**, 514 (1995).
[14] W. J. Witteman, *The CO_2 Laser* (Springer-Verlag, New York, 1987).
[15] F. Nez, M. Plimmer, S. Bourzeix, L. Julien, F. Biraben, R. Felder, O. Acef, J. Zondy, P. Laurent, A. Clairon, M. Abed, Y. Millerioux, and P. Juncar, Phys. Rev. Lett. **69**, 2326 (1992).
[16] M. Weitz, A. Huber, F. Schmidt-Kaler, D. Leibfreid, and T. Hänsch, Phys. Rev. Lett. **72**, 328 (1994).
[17] G. D. Stevens, C.-H. Iu, T. Bergeman, H. J. Metcalf, I. Seipp, K. T. Taylor, and D. Delande, Phys. Rev. A **53**, 1349 (1996), Appendix.
[18] G. W. F. Drake and R. Swainson, Phys. Rev. A **44**, 5448 (1991).
[19] M. L. Zimmerman, M. G. Littman, M. M. Kash, and D. Kleppner, Phys. Rev. A **20**, 2251 (1979).
[20] S. Bhatti, C. Cromer, and W. Cooke, Phys. Rev. A **24**, 161 (1981).
[21] R. R. Freeman and D. Kleppner, Phys. Rev. A **14**, 1614 (1976).
[22] C. Fabre, M. Gross, and S. Haroche, Opt. Commun. **13**, 393 (1975).
[23] C. Fabre, Ann. Phys. (Paris) **7**, 247 (1982).
[24] S. Dyubko, V. Efremov, S. Podnos, X. Sun, and K. B. MacAdam, J. Phys. B **30**, 2345 (1997).